Self-Assembled Triple-Stranded Lanthanide Dimetallic Helicates with a Ditopic Ligand Derived from Bis(benzimidazole)pyridine and Featuring an (4-Isothiocyanatophenyl)ethynyl Substituent

by **Raphaël Tripier**[a]), **Marcel Hollenstein**[a]), **Mourad Elhabiri**[a]), **Anne-Sophie Chauvin**[a]), **Gaël Zucchi**[a]), **Claude Piguet**[b]), and **Jean-Claude G. Bünzli***[a])

[a]) Swiss Federal Institute of Technology Lausanne, Institute of Molecular and Biological Chemistry, BCH 1402, CH-1015 Lausanne (e-Mail: jean-claude.bunzli@epfl.ch)

[b]) Department of Inorganic, Analytical and Applied Chemistry, University of Geneva, 30 quai E. Ansermet, CH-1211 Geneva 4

Bis(2-{6-(diethylcarbamoyl)-4-[(4-isothiocyanatophenyl)ethynyl]pyridin-2′-yl}-1-ethylbenzimidazol-5-yl)-methane ($\mathbf{L^G}$) reacts with trivalent lanthanide ions in acetonitrile to yield triple-stranded dimetallic helicates $[Ln_2(\mathbf{L^G})_3]^{6+}$. ^{1}H-NMR Data point to the helicates being the only species formed under stoichiometric conditions and having a time-averaged D_3 symmetry on the NMR time scale. The photophysical properties of $\mathbf{L^G}$ and its helicates are discussed with respect to the closely related ligands $\mathbf{L^B}$, $\mathbf{L^E}$, and their complexes, two ligands devoid of the isothiocyanatophenylethynyl substituent. The quantum yield of the ligand fluorescence is three times smaller compared to $\mathbf{L^E}$, while that of the Eu^{III}-centered luminescence (1.1%) is three times larger. On the other hand, the luminescence of Tb^{III} is not sensitized by $\mathbf{L^G}$. This is explained in terms of energy differences between the singlet and triplet states on one hand, and between the 0-phonon transition of the triplet state and the excited metal ion states on the other. This work demonstrates that bulky substituents in the 4-position of the pyridine ring do not prevent the formation of triple-stranded helicates, opening the way for luminescent probes that can easily be coupled to biological materials.

Introduction. – Supramolecular functional architectures containing lanthanide ions receive a sustained interest, especially in the field of medicine, because the optical and magnetic properties arising from the shielded 4f electronic configurations are easily traceable, therefore, providing suitable diagnostic [1][2], therapeutic [3][4], or analytical tools [5][6]. One challenge associated with the development of such molecular edifices lies in the accurate control of the Ln^{III} inner coordination sphere in order to reach large thermodynamic stability and kinetic inertness without altering the specific properties of the metal ion. In the particular case of photophysical properties, additional features have to be incorporated in the receptor in order to achieve efficient sensitization of the luminescent lanthanide ions [7]. In recent years, we have focused part of our research efforts on the design of segmental ligands featuring aromatic tridentate and/or bidentate coordination units and coded for the self-assembly of 4f-4f [8] or 4f-3d [9][10] dimetallic helicates. We have shown that the coordination sphere of the Ln^{III} ions can be controlled by semirigid aromatic tridentate ligands such as bis(benzimidazole)pyridines [11][12]. The covalent connection of two such units leads, for example, to the formation of ditopic ligand $\mathbf{L^A}$ (*Scheme 1*), forming stable dimetallic helicates $[Ln_2(\mathbf{L^A})_3]^{6+}$ in MeCN in which the ligand strands are wrapped around two 9-coordinate Ln^{III} ions with tricapped trigonal prismatic coordination geometry [13][14]. The self-assembly process results in the formation of protective

environments for the metal ions, with the ligand strands wrapped tightly around them and held together by weak interstrand π-π stacking interactions [14]. To increase the resistance of the molecular edifices toward hydrolysis, we have modified the terminal subunits of ligand $\mathbf{L^A}$ by introducing dialkylamide groups (*cf.* $\mathbf{L^B}$) [15]. Further hydrolysis of the amide functions resulted in a dicarboxylic ligand $\mathbf{L^C}$ inducing the self-assembly of neutral and highly stable $[Ln_2(\mathbf{L^C}\text{-}2\,H)_3]$ helicates in H_2O [16]. The use of magnetic (*e.g.*, in magnetic resonance imaging [2]) or luminescent (*e.g.*, in fluoroimmunoassays [5]) lanthanide-containing probes frequently requires a coupling with the biological material of interest, for instance, monoclonal antibodies. Such bioconjugates are often obtained by reacting the amine functions of the antibody with isothiocyanate (SCN) groups located on the metal chelate and held at a reasonable distance from the active site of the probe [17]. In this paper, we build on our recent work in which halogen substituents were introduced at C(4) of the pyridine moieties of $\mathbf{L^B}$ to yield the reactive synthons $\mathbf{L^E}$ and $\mathbf{L^F}$ [18]. The latter are used to introduce a (4-isothiocyanatophenyl)-ethynyl substituent at C(4) of pyridine (*cf.* $\mathbf{L^G}$), a group known for its easy coupling with amino functions of antibodies [5], oligonucleotides and proteins in the case of DNA labelling [19][20]. The aim of the paper is to test the influence of these relatively bulky groups on the wrapping process around the lanthanide ion and on the photophysical properties of the resulting assemblies.

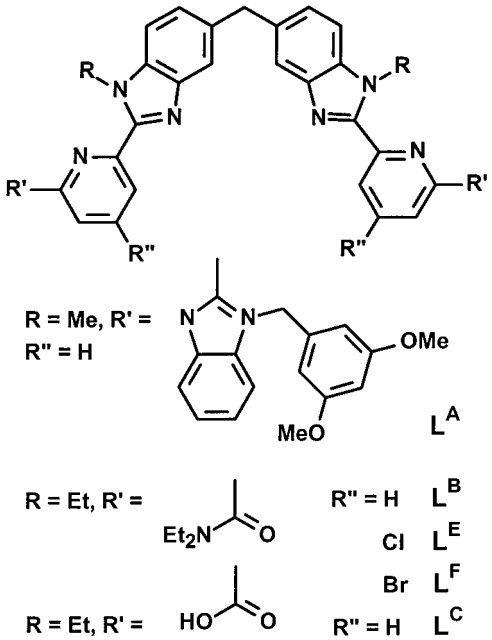

Results and Discussion. – *Synthesis and Solution Structure of Ligand* $\mathbf{L^G}$. Bis(2-{6-(diethylcarbamoyl)-4-[(4-isothiocyanatophenyl)ethynyl]pyridin-2-yl}-1-ethyl benzimidazol-5-yl)methane ($\mathbf{L^G}$) was obtained in good yield according to the previously described two-step procedure, relying on a modified *Phillips* coupling reaction as the key step in achieving the desired benzimidazole units. One of the starting materials is

the analogous 4-halogenated compound ($\mathbf{L^E}$ or $\mathbf{L^F}$, X = Cl or Br) synthesized according to the improved procedure we have recently proposed [21]. The halogen functions at C(4) of the pyridine were first substituted by (4-aminophenyl)ethyne moieties (*Scheme 1*) according to a modification of *Heck*'s coupling reaction [22] reported by *Sonogashira et al.* [23]. (4-Aminophenyl)ethyne itself was synthesized *via* a literature

Scheme 1

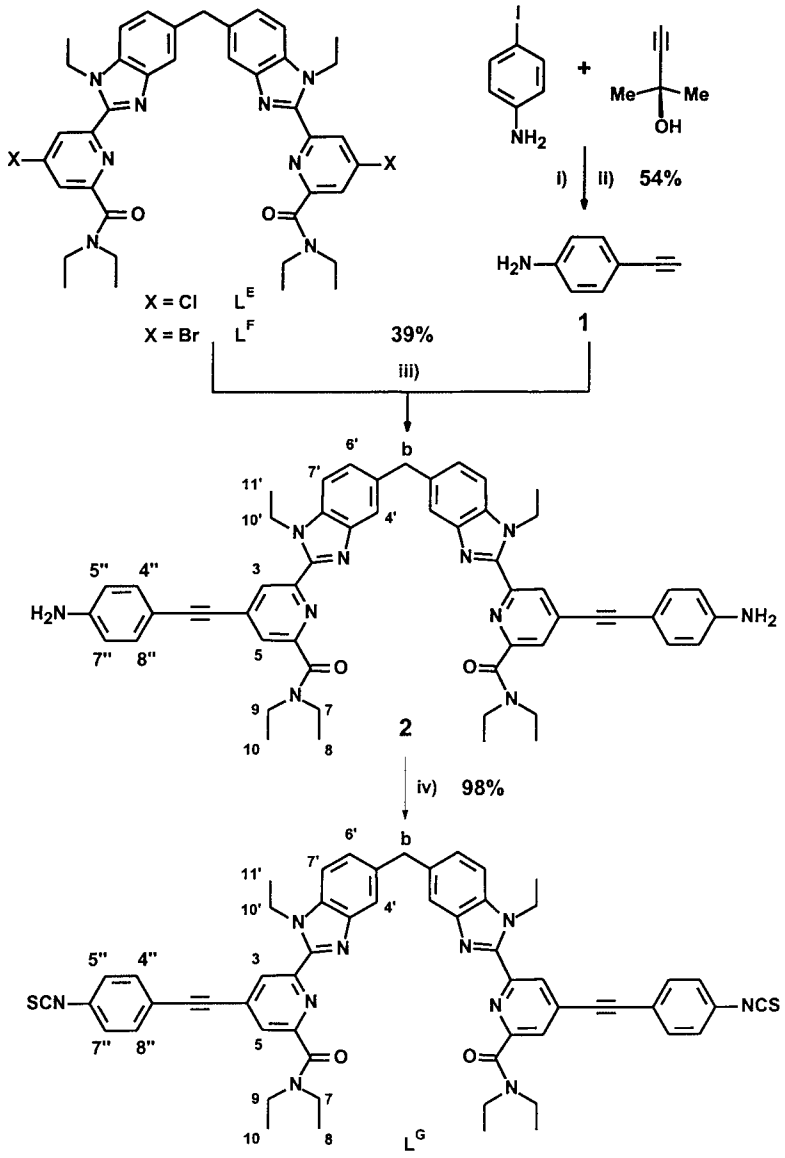

i) $[PdCl_2(PPh_3)_2]$, CuI, Et_3N. ii) NaOH. iii) **1**, $[PdCl_2(PPh_3)_2]$, CuI, Et_3N/THF. iv) DPT, CH_2Cl_2.

procedure [24] in a somewhat better yield (54 instead of 43%), similar to the yield reported by *Mongin* and *Gossauer* (57%) [25]. Our choice of this method over the more efficient one proposed by *Lavastre et al.* (71%) [26] was dictated by the milder reaction conditions and lower cost of the starting materials. The NH_2 functions were subsequently transformed into SCN groups with di(pyridin-2-yl)thiocarbonate (DPT), a reagent far less toxic than thiophosgene. The reactivities of the two halogen substituents analogues were compared and, surprisingly, it appeared that the brominated synthon $\mathbf{L^F}$ reacts less readily than chlorinated $\mathbf{L^E}$, the yields being 28 and 39%, respectively. This may be due to poor solubility of $\mathbf{L^F}$ under the conditions used. The yield obtained with the chlorinated derivative is in the range of those reported for similar coupling reactions [27]. The IR spectrum of $\mathbf{L^G}$ presents an intense C=O stretching band at 1636 cm^{-1} arising from the amide group, a value close to that obtained for the C=O groups of $\mathbf{L^B}$. These observations point to the environment of the amide group being probably not much modified by the 4-substitution of the pyridine unit. A broad band at 2039 cm^{-1} is assigned to the antisymmetric stretching of the SCN groups.

The solution structure of $\mathbf{L^G}$ in $CDCl_3$ was investigated by ^{1}H- (*Fig. 1* and *Table 1*) and ^{13}C-NMR spectroscopy, including ^{1}H-^{1}H COSY and ^{1}H-^{13}C (HSQC) experiments that allowed us to assign all observed signals. The spectra are typical of a species with C_{2v} symmetry (14 peaks for the 50 protons of the molecule and 25 peaks for the 57 C-atoms – two pairs of signals overlap accidentally. To assess the arrangement of the terdentate coordinating units, ROESY (*R*otating frame *O*verhauser *E*nhancement *S*pectroscop*Y*) experiments were carried out on a solution of $\mathbf{L^G}$ in $CDCl_3$. Along with

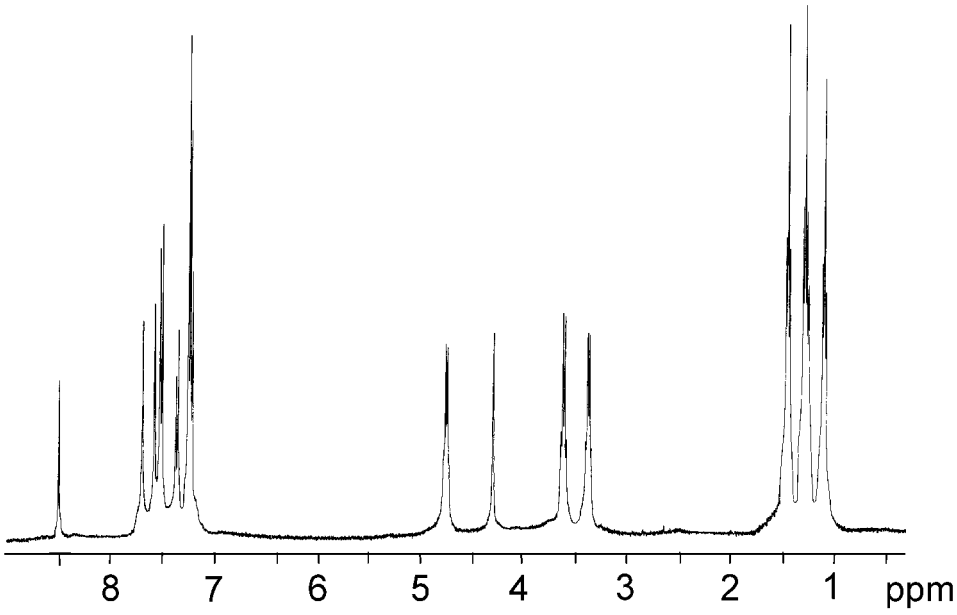

Fig. 1. *^{1}H-NMR Spectrum of [$La_2(\mathbf{L^G})_3$]$^{6+}$* ($CDCl_3$, 400 MHz, 295 K)

Table 1. *^{1}H-NMR Chemical Shifts* (δ, with respect to TMS) *for* $\mathbf{L^G}$ ($CDCl_3$) *and Chemical-Shift Differences* $\Delta\delta = \delta_{compl} - \delta_{lig}$ [ppm] *for* $[Ln_2(\mathbf{L^G})_3]^{6+}$ (Ln = Eu, La, (CD_3CN), at 295 K and 400 MHz)

		H–C(3)	H–C(4′)	H–C(5)	H–C(5″), H–C(7″)	H–C(7′)	H–C(4″), H–C(8″)	H–C(6′)
$\mathbf{L^G}$	δ/ppm	8.51	7.70	7.59	7.53	7.37	7.24	7.22
	mult.	*d*, 1 H	*s*, 1 H	*d*, 1 H	*d*, 2 H	*d*, 1 H	*s*, 2 H	*s*, 1 H
Eu	$\Delta\delta$/ppm[a])	− 3.25	5.19	− 2.09	− 0.05	0.51	0.09	− 0.74
	mult.	*s*, 1 H	*s*, 1 H	*s*, 1 H	*dd*, 2 H	*d*, 1 H	*dd*, 2 H	*d*, 1 H
	J/Hz				2.1, 6.6	8.7	2.1, 6.8	8.5
La	$\Delta\delta$/ppm	− 0.30	− 1.69	0.02	− 0.04	0.06	− 0.01	+ 0.02
	mult.	*d*, 1 H	*s*, 1 H	*d*, 1 H	*dd*, 2 H	*d*, 1 H	*dd*, 2 H	*d*, 1 H
	J/Hz	0.8		0.8	1.9, 6.4	8.4	1.9, 6.4	7.8
		CH_2(b)	H–C(10′)	H–C(7)	H–C(9)	H–C(11′)	H–C(8)	H–C(10)
$\mathbf{L^G}$	δ/ppm	4.30	4.76	3.62	3.38	1.45	1.29	1.10
	mult.	*s*, 1 H	*q*, 2 H	*q*, 2 H	*q*, 2 H	*t*, 3 H	*t*, 3 H	*t*, 3 H
Eu	$\Delta\delta$/ppm	0.28	− 1.06	0.45	− 0.41	2.11	− 0.58	− 0.71
	mult.	*s*, 1 H	*m*, 2 H	*m*, 2 H	*m*, 2 H	*t*, 3 H	*t*, 3 H	*t*, 3 H
	J/Hz					5.8	7.1	7.0
La	$\Delta\delta$/ppm	− 0.38	− 0.02	− 0.11	− 0.39	0.06	− 0.28	− 0.18
	mult.	*s*, 1 H	*m*, 2 H	*m*, 2 H	*m*,2 H	*t*, 3 H	*t*, 3 H	*t*, 3 H
	J/Hz					7.0	7.1	6.8

[a]) $\Delta\delta = \delta_{complex} - \delta_{ligand}$.

the results of a COSY investigation, this experiment clearly points to a *transoid* conformation of the terminal pyridines with respect to the benzimidazole moieties. NOE Effects are found between the bridging CH_2(b) H-atoms and H–C(4′), H–C(6′) as well as between H–C(10′) and H–C(7′). No such effect is detected between H–C(10′) and the aromatic H-atoms of the pyridine unit. The C_{2v} symmetry and the *transoid* conformation are further supported by the molecular-mechanics optimization performed with the program HyperChem [28] (*Fig. 2*).

Formation of the Dimetallic Helicates. Reaction of stoichiometric amounts of $\mathbf{L^G}$ and $Ln(ClO_4)_3 \cdot x\,H_2O$ (Ln = La, Eu, Tb) in an $MeCN/CH_2Cl_2$ mixture gave pale yellow solutions, from which the complexes $[Ln_2(\mathbf{L^G})_3](ClO_4)_6 \cdot n\,H_2O$ ($n = 3-6$) were recrystallized in 65–70% yields. The IR spectra of these helicates present a number of identifying bands including *i*) an intense C=O stretching vibration at 1581 cm^{-1}, red shifted by 55 cm^{-1} with respect to $\mathbf{L^G}$ and indicating a strong Ln^{III}-amide interaction, *ii*) intense stretching vibrations at 2088 and 2208 cm^{-1} arising from the isothiocyanate and C≡C groups, respectively, the vibration mode of the SCN groups being blue-shifted by 49 cm^{-1} with respect to $\mathbf{L^G}$, *iii*) a broad band at 3400 cm^{-1} arising from interstitial H_2O molecules, and *iv*) vibrations from ionic perchlorate at 1090 and 624 cm^{-1}.

The ^{1}H-NMR spectra of the La^{III} and Eu^{III} helicates (*Table 1*) show an A_2 spin system for the bridging CH_2 group, which is typical for two C_2-related homotopic protons, while the *AB* spin system observed for CH_2(10′) arises from two diastereotopic protons, thus indicating a time-averaged D_3 symmetry in solution on the NMR time-scale. As previously observed with $\mathbf{L^A}$, $\mathbf{L^B}$, and $(\mathbf{L^C}\text{-}2\,H)^{2-}$ the signal of the H-atoms at C(4′) is the most shifted upon complexation because wrapping the ligands around the metal ions brings them *i*) into the shielding region of the neighboring benzimidazole

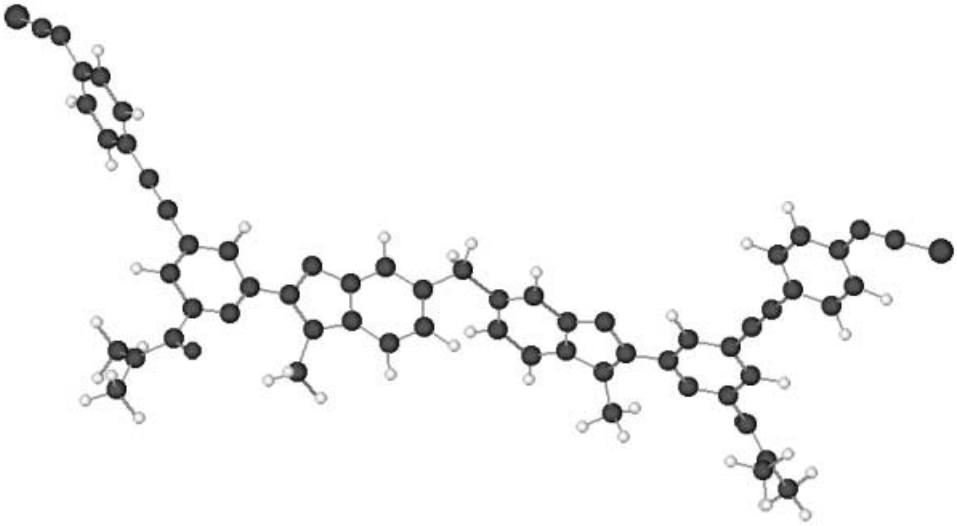

Fig. 2. *Optimized geometry of* $\mathbf{L^G}$ *obtained by molecular mechanics*

ring and *ii*) close to the metal centers, a crucial effect for pseudo-contact shifts with paramagnetic Eu^{III} [14][15]. The pyridine H–C(3) and H–C(5) also undergo substantial shifts as a result of *i*) the coordination of the N-atom to the metal ions and *ii*) the conformational change from a *transoid* to a *cisoid* arrangement of the two ligand arms, as confirmed by the NOE effect detected between H–C(10′) and H–C(3). A comparison with the NMR spectra of $[Ln_2(\mathbf{L^B})_3]^{6+}$ and $[Ln_2(\mathbf{L^E})_3]^{6+}$ leads to the conclusion that the complexes with $\mathbf{L^B}$, $\mathbf{L^E}$, and $\mathbf{L^G}$ adopt a similar helical conformation, whatever the nature and bulkiness of the substituent at C(4) of the pyridine. Moreover, it appears that the ionic-radius contraction does not modify substantially the overall structure of the helicates. In the helicates with $\mathbf{L^B}$ and $\mathbf{L^E}$, the protons $CH_2(7)$, $CH_2(9)$, and $CH_2(10')$ are diastereotopic at room temperature [15][18] (six signals observed), due to a blocked D_3 triple helical structure. In the case of $\mathbf{L^G}$, the corresponding signals overlap indicating a less different micro-environment and slightly different wrapping of the ligands in $[Ln_2(\mathbf{L^G})_3]^{6+}$ (*Table 1*). On the other hand, the aromatic protons of the (4-isothiocyanatophenyl)ethynyl substituent are only slightly influenced upon complexation ($\Delta\delta \approx 0.07$ ppm, Eu helicate with $\mathbf{L^G}$). It is noteworthy that a more pronounced effect was observed with triple-helical mononuclear complexes with 4-[(4-aminophenylenyl)ethynyl]pyridine-2,6-dicarboxylic acid, $[LnL_3]^{3+}$ [29].

To find out whether other species form during the self-assembly process, we have titrated $\mathbf{L^G}$ with $Eu(ClO_4)_3 \cdot x\ H_2O$ and monitored the resulting solutions by ^{1}H-NMR for ratios $R = [Eu^{III}]_{tot}/[\mathbf{L^G}]_{tot}$ between 0.25 and 1. For $R \leq 0.5$, the spectra show the presence of the free ligand and of the 2:3 complex, but no other species could be detected. When R reaches 0.67, the signals are identical to those observed for the isolated complex $[Eu_2(\mathbf{L^G})_3]^{6+}$. This experiment, therefore, unambiguously indicates the formation of the thermodynamically stable 2:3 helicate by strict self-assembly,

under stoichiometric conditions and high ligand concentration. When $R > 0.67$, other signals appear that may tentatively be assigned to a 2:2 species [15].

Photophysical Properties in Solution: Ligand-Centered Transitions. The absorption spectrum of **L^G** in MeCN at room temperature presents two broad bands in the range 25 – 45000 cm^{-1}, which were assigned to $\pi \rightarrow \pi^*$ transitions (*Fig. 3* and *Table 2*). The band centered at 31570 cm^{-1} is comprised of four components and is typical of an extended aromatic system. Comparison with the spectra of similar and model molecules (**L^1** and **L^2**; *Scheme 2*) leads to the following assignment. The components at 28310 and 30400 cm^{-1} correspond to transitions mainly centered onto the pyridine and benzimidazole units, while the component at 31570 cm^{-1} appears to be typical of the (4-isothiocyanatophenyl)ethynyl group. With respect to **L^E**, the envelope of the first absorption band is slightly shifted towards higher energies. On the other hand, in frozen MeCN solution, the energy of the singlet state of **L^G** is red-shifted by *ca.* 4000 cm^{-1} compared to **L^E**, while the 0-phonon component of the triplet state is less sensitive to the substitution at C(4) of the pyridine, its energy being 20090 cm^{-1}, compared to 21200 and 21280 cm^{-1} for **L^E** and **L^B**, respectively. It has been suggested that an efficient intersystem crossing occurs, when the energy difference between the singlet and triplet states amounts to *ca.* 5000 cm^{-1} [30]. This is an important factor in the sensitization of lanthanide ions, since the ligand-to-metal energy-transfer process will be more efficient when the triplet-state population is larger. For **L^E**, $\Delta E(^1\pi\pi^* - {}^3\pi\pi^*) \approx 4700$ cm^{-1} [18] (taken as the energy difference between the maximum of the fluorescence band and the 0-phonon component of the triplet state), while this value is smaller for both **L^B** (*ca.* 3000 cm^{-1}) [15] and **L^G** (*ca.* 2090 cm^{-1}), resulting in a quite weak triplet-state emission, which is seen only at low temperature. Other differences in the photophysical properties of **L^E** and **L^G** lie in their fluorescence quantum yields and in the lifetimes of

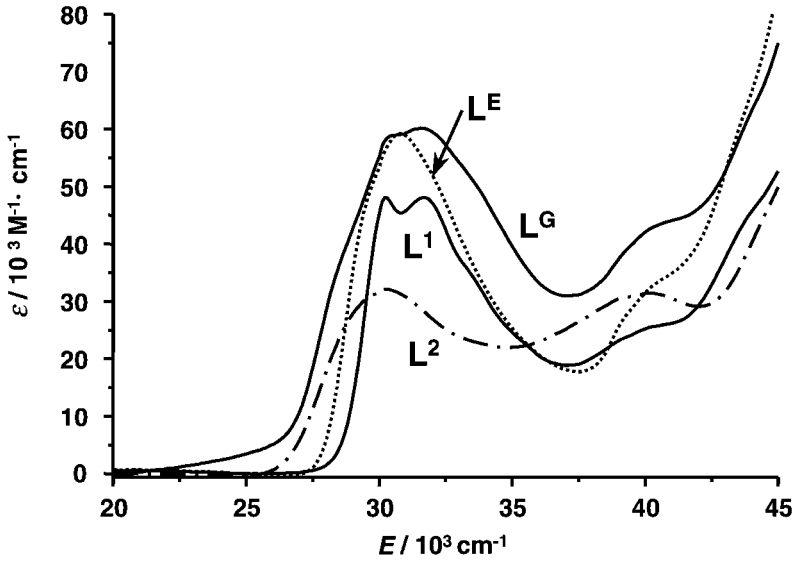

Fig. 3. *Absorption spectra of ligands* **L^E**, **L^G**, **L^1** *and* **L^2** ($7-8\cdot10^{-7}$ M in MeCN at 295 K).

Table 2. *Ligand-Centered Absorption and Emission Properties of the Ligand* $\mathbf{L^G}$ *and* $[Ln_2(\mathbf{L^G})_3]^{6+}$ (Ln = La, Eu, Tb). Data for $\mathbf{L^B}$ and $\mathbf{L^E}$ are taken from [15] and [18], respectively.

Compound	$E(\pi \rightarrow \pi^*)$/cm^{-1}[a])	$E(^1\pi\pi^*)$/cm^{-1}[b])	$E(^3\pi\pi^*)$/cm^{-1}[b])	$\tau(^3\pi\pi^*)$/ms[b])
$\mathbf{L^B}$	*32200*	24330[c])	19940 (sh)[c])	4.2 ± 0.2
	41320 (sh)		*20040*[b])	
			21280 (sh)[c])	
$\mathbf{L^E}$	29420 (sh)	25880	16810 (sh)	670 ± 20
	30840		18000 (sh)	
	40160 (sh)		*18960*	
			21200	
$\mathbf{L^G}$	28310 (sh)	22170	17400 (sh)	171 ± 3
	30400		*18470*	
	31570		20090	
	32750 (sh)			
	40140 (sh)			
$[La_2(\mathbf{L^G})_3]^{6+}$	*28420*	22420	18380	537 ± 30
	34120 (sh)		18900	
	40120 (sh)		19800	
$[Eu_2(\mathbf{L^G})_3]^{6+}$	*28340*	20620		
	34140 (sh)		[d])	[d])
	43460 (sh)			
$[Tb_2(\mathbf{L^G})_3]^{6+}$	*28390*	21050	16250	570 ± 50
	34210 (sh)		16950	
	43460 (sh)		17940	
$\mathbf{L^1}$	*30260*	23550	18420[c])	560 ± 10[c])
	31730		*19600*[c])	
	33740 (sh)		20780[c])	
	40000 (sh)			
$\mathbf{L^2}$	*30270*	23240	19100[c])	159 ± 4[c])
	40170 (sh)		*20190*[c])	
			21280[c])	

[a]) Electronic spectral data at 295 K in MeCN; energies are given for the maximum of the band envelope (sh: shoulder). [b]) Luminescence data in MeCN at 77 K. [c]) Solid-state luminescence data at 77 K. [d]) $^3\pi\pi^*$ Luminescence quenched by transfer to the Eu ion. Values in *italics:* maximum of the absorption bands.

their triplet states. In MeCN, the absolute fluorescence quantum yield of $\mathbf{L^G}$ amounts to 24%, compared to 92% for $\mathbf{L^E}$ [18], and at 77 K the $\tau(^3\pi\pi^*)$ lifetime is concomitantly smaller (171 ms) than for $\mathbf{L^E}$ (670 ms) [18]. A first conclusion is that nonradiative deactivation pathways are more effective in $\mathbf{L^G}$ compared to $\mathbf{L^E}$ probably because of the more-extended π-system of the former.

Photophysical Properties in Solution: $[Ln_2(L^G)_3]^{6+}$ *Helicates (Ln = La, Eu, Tb).* In MeCN, the dimetallic helicates display three absorption bands centered around 28400, 34000, and 43500 cm^{-1} (*Table 2*). The 30400-cm^{-1} absorption band of uncomplexed $\mathbf{L^G}$ split upon complexation, one component appearing at lower energy (*ca.* 2000 cm^{-1}, similar to the shift observed for $[Ln_2(\mathbf{L^B})_3]^{6+}$ [15]), while the other component undergoes an hypsochromic shift of *ca.* 3000 cm^{-1}.

Upon ligand excitation, one broad fluorescence band is seen for all the investigated complexes. In MeCN at 77 K, the energy shift of the $^1\pi\pi^*$ state with respect to uncomplexed $\mathbf{L^G}$ amounts to 250, 1550, and 1120 cm^{-1} for La, Eu, and Tb, respectively.

Scheme 2

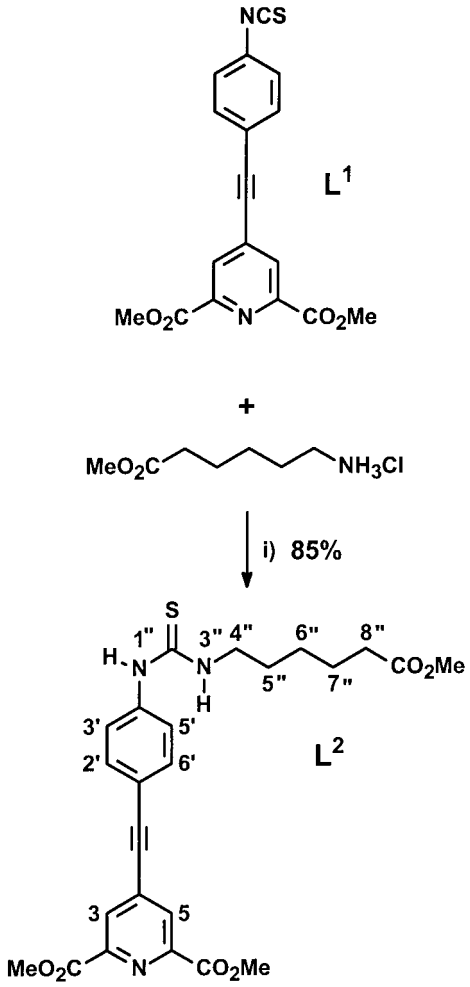

i) MeCN, $NaHCO_3$, r.t.

This shift is much smaller than those observed for the helicates prepared from $\mathbf{L^E}$ (3150 to 3640 cm^{-1} from La to Lu), consistent with the fairly different electronic structure of the two ligands. A bathochromic shift is observed for the 0-phonon component of the $^3\pi\pi^*$ emission band at 77 K: 290 and 2150 cm^{-1} for La and Tb, respectively. The triplet-state emission is not seen for the Eu helicate, but, instead, the characteristic metal-centered $^5D_0 \rightarrow {}^7F_J$ emission lines appear, pointing to an efficient $^3\pi\pi^*$ state-to-metal ion energy transfer. On the other hand, Tb^{III} luminescence is not sensitized (*Fig. 4*) because the energy of the triplet state (17940 cm^{-1}) is smaller than the energy of the $^5D_4$ level (*ca.* 21000 cm^{-1}). The lifetime of the ligand $^3\pi\pi^*$ states is much larger in the helicates, which, besides the heavy-atom effect, points to the ligand conformation being rigidified upon complexation.

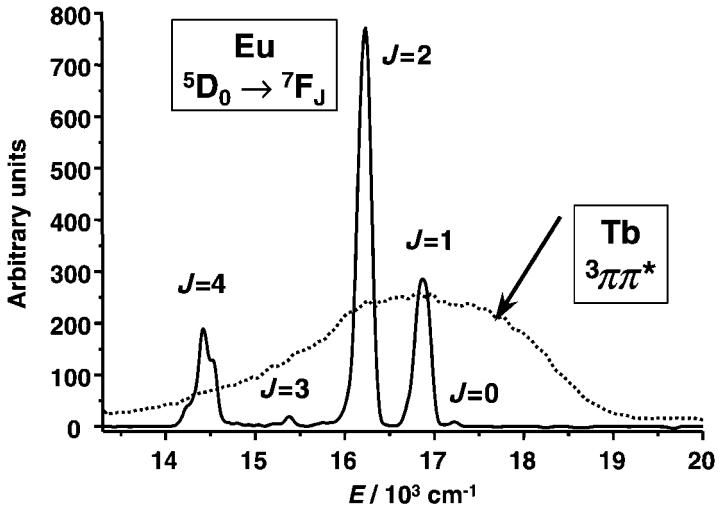

Fig. 4. *Phosphorescence spectra of* $[Ln_2(\mathbf{L^G})_3]^{6+}$ (Ln = Eu, Tb) *in frozen* MeCN *at 77 K* ($\tilde{\nu}_{exc} = 25640$ (Eu) and 25455 (Tb) cm^{-1})

The absolute quantum yield of $[Eu_2(\mathbf{L^G})_3]^{6+}$ has been measured in MeCN solution. It amounts to 1.1%, a value three times larger than the ones reported for the helicates with $\mathbf{L^B}$ (0.35%) [15] and $\mathbf{L^E}$ (0.45%) [18]. The overall sensitization of the lanthanide ion luminescence is proportional to the product of the efficiencies of intersystem crossing and of the $^3\pi\pi^*$-to-Ln^{III} transfer. The former energy-transfer process is not very efficient, mainly due to a small energy difference between the singlet and triplet state (*ca.* 2090 cm^{-1} for $\mathbf{L^G}$ and 2620 cm^{-1} for $[La_2(\mathbf{L^G})_3]^{6+}$). The second process may be quite complex, involving several metal-ion excited states (and the ligand $^1\pi\pi^*$ state) [31] and depending on *i*) the relative energy of the ligand and metal-ion excited states, and *ii*) the donor-acceptor distance and the orientation of the chromophore (donor) with respect to the metal ion (acceptor) [32]. In our case, the energetic factor, $\Delta E(^3\pi\pi^* - {}^5D_0)$, is not favorable: as a rule of thumb, an energy difference of *ca.* 2000–2500 cm^{-1} is considered to be optimum, since it minimizes back-transfer processes [30][33]. Substitution at C(4) brings $\Delta E(^3\pi\pi^* - {}^5D_0)$ from *ca.* 3700 cm^{-1} for $\mathbf{L^B}$ (measured on the Gd helicate) to *ca.* 3220 cm^{-1} for $\mathbf{L^E}$ (measured on the Gd helicate) and to only *ca.* 2600 cm^{-1} (measured on the La helicate) for $\mathbf{L^G}$. Therefore, the larger quantum yield of $[Eu_2(\mathbf{L^G})_3]^{6+}$ arises either from better orientation of the chromophoric antenna or from reduced nonradiative deactivation processes. For Eu^{III} compounds, photoelectron-transfer processes and ligand-to-metal charge-transfer state(s) must also be taken into account. The luminescence lifetime of the $^5D_0$(Eu) level gives some clue to this problem. First, it is quite large at room temperature, *e.g.*, 2.02 ± 0.01 ms in the solid state and 1.62 ± 0.01 ms in MeCN; therefore, reflecting the absence of high-energy oscillators (*e.g.*, OH) in the inner coordination sphere of the metal ion. The latter value is similar to those found for the helicates with $\mathbf{L^B}$ (1.67 ms [15]) and $\mathbf{L^E}$ (1.60 ms [18]), illustrating that, in solution, the Eu^{III} coordination sphere is comparable for the three helicates, the helical wrapping of the ligand strands providing good protection of the metal ions against solvent interaction. The temperature

dependence of the lifetime is also similar for the three helicates: for anhydrous solid-state samples of $[Eu_2(\mathbf{L^B})_3]^{6+}$ and $[Eu_2(\mathbf{L^E})_3]^{6+}$, $\tau(^5D_0)$ decreases from 2 ms (77 K) to 1.6 ms (295 K) [15], and from 2.2 (77 K) to 1.5 ms (295 K), respectively [18], while a decrease from 1.8 (77 K) to 1.6 ms (295 K) is observed for $[Eu_2(\mathbf{L^G})_3]^{6+}$ in MeCN. Therefore, temperature-dependent deactivation processes are similar for the three helical molecular edifices. This is surprising in view of the small $\Delta E(^3\pi\pi - {}^5D_0)$ value for the $\mathbf{L^G}$ helicate. The larger quantum yield observed for $[Eu_2(\mathbf{L^G})_3]^{6+}$ has, therefore, to be explained by a more favorable positioning of the chromophore.

Photophysical Properties of $[Eu_2(\mathbf{L^G})_3]^{6+}$ in the Solid State. We have taken advantage of the Eu^{III} luminescence to probe the environment of the metal ion, despite the relative broadness of the emission bands. Upon excitation through the ligand $^1\pi\pi^*$ state at 295 K, the emission spectrum displays the characteristic $Eu(^5D_0 \rightarrow {}^7F_J)$ transitions. The crystal-field splitting of the spectrum can be interpreted in terms of a coordination polyhedron derived from D_3 symmetry. The extremely weak and broad $^5D_0 \rightarrow {}^7F_0$ transition is consistent with the fact that it is symmetry forbidden in the D_3 symmetry point group. The $^5D_0 \rightarrow {}^7F_1$ transition displays three components (*Table 3*), corresponding to $^5D_0(A_1) \rightarrow {}^7F_1(A_2)$ and to a $^5D_0(A_1) \rightarrow {}^7F_1$(split E-sublevel), which are both allowed in D_3 symmetry; the splitting amounts to 43 cm^{-1}, reflecting a relatively large distortion from D_3 symmetry. For comparison, splittings in the range 20–30 cm^{-1} and 60–75 cm^{-1} were observed for the helicates with $\mathbf{L^B}$ and $\mathbf{L^E}$, respectively. The $^5D_0 \rightarrow {}^7F_2$ transition is the most intense (1.9 times the intensity of the $^5D_0 \rightarrow {}^7F_1$ transition) and displays five bands; two *doublets* are assigned to the allowed transitions $A_1 \rightarrow E$ in D_3 symmetry (splittings of 27 and 29 cm^{-1}). Analysis of the $^5D_0 \rightarrow {}^7F_4$ transition shows six components, two appearing as closely spaced *doublets* (three transitions to E sublevels and one to an A_2 sublevel are allowed in D_3): the less intense *singlet* at 14146 cm^{-1} is assigned to the $A_1 \rightarrow A_2$ transition, and the broad one at 14401 cm^{-1} to one $A_1 \rightarrow E$ transition. The two *doublets* are assigned to two $A_1 \rightarrow E$ transitions (splitting of 41 and 38 cm^{-1}). In conclusion, the solid-state structure of the Eu helicate is similar to those determined for the complexes with $\mathbf{L^B}$ and $\mathbf{L^E}$, and comparable to the solution structure unravelled by the NMR investigation.

Table 3. *Electronic Sublevels* ([cm^{-1}], origin: $^5D_0$) *of the Eu(^7F_J) Manifold* ($J = 1-4$) *in $[Eu_2(\mathbf{L^G})_3]^{6+}$ as Determined from Emission Spectra in the Solid State at 295 K*

$^5D_0$	$^7F_1$	$^7F_2$	$^7F_3$	$^7F_4$
17222	319	981	1833	2690
	380	1008		2731
	423	1050		2821
		1076		2987
		1107		3025
				3076

Conclusions and Perspectives. – The introduction of (4-isothiocyanatophenyl)-ethynyl groups at C(4) of the pyridine rings of ligand $\mathbf{L^B}$ is easily achieved, and the resulting functionalized ditopic and hexadentate ligand $\mathbf{L^G}$ is obtained in reasonable overall yield, 38%, as calculated from $\mathbf{L^E}$ and **1**, itself obtained in 38% yield [21]. Under

stoichiometric conditions, $\mathbf{L^G}$ self-assembles with lanthanide perchlorates in MeCN to yield dimetallic triple-stranded helicates $[Ln_2(\mathbf{L^G})_3]^{6+}$ in 65–71% yield. NMR Spectra show the structures of these molecular edifices in comparison to those of the analogous helicates with $\mathbf{L^A}$ [14], $\mathbf{L^B}$ [15], and $\mathbf{L^E}$ [18]. We, thus, deduce that the bulky substituents at C(4) of pyridine do not prevent helical wrapping of the ligand strands around the metal ions. The electron-withdrawing substituents provide a moderate antenna effect for Eu^{III}, with a threefold increase in the quantum yield of the metal-centered luminescence as compared with helicates with $\mathbf{L^B}$ and $\mathbf{L^E}$. On the other hand, the (4-isothiocyanatophenyl)ethynyl substituents induce a bathochromic shift of the ligand triplet state that lies at an energy too low to sensitize the luminescence of Tb^{III}.

In conclusion, we have demonstrated that the ligands $\mathbf{L^{A–G}}$ represent a versatile class of ditopic receptors, amenable to easy substitution while retaining their coordination properties for the self-assembly of triple-stranded lanthanide-containing helicates. The choice of introducing two equivalent binding points in $\mathbf{L^G}$ has mainly been dictated by a simpler synthetic chore and because a symmetrical ligand generates simple NMR spectra. In view of the results obtained, work is in progress to improve the sensitization properties of these receptors, to replace the diethylamide function by carboxylic groups, as well as to introduce a single isothiocyanate group and test the coupling reactions of the helicates with biological material.

Experimental Part

General. MeCN, CH_2Cl_2, DMF, and Et_3N were distilled from CaH_2; $SOCl_2$ was distilled from elemental S. Silica gel (Merck *60*, 0.04–0.06 mm) was used for prep. column chromatography (CC). Other products were purchased from *Fluka AG* (Buchs, Switzerland) and used without further purification, unless otherwise stated.

Spectroscopic and Analytical Measurements. Electronic spectra in the UV/VIS range were recorded at 20° with a *Perkin-Elmer Lambda 7* spectrometer in 1.0- and 0.1-cm quartz cells. IR Spectra were obtained from KBr pellets with a *Mattson α-Centauri* FT-IR spectrometer. ES-MS spectra of the complexes were measured on a *Finnigan SSQ-710C* spectrometer on 10^{-4} M solns. in MeCN; the cap. temp. was set to 200° and the acceleration potential to 4.5 kV. ^{1}H- and ^{13}C-NMR spectra were recorded at 25° on *Bruker AM-360* or *Bruker AVANCE 400-DRX* spectrometers. Chemical shifts are reported in ppm with respect to TMS; *J* values are given in Hz. Solns. for the titration of $\mathbf{L^G}$ by $Eu(ClO_4)_3 \cdot x\ H_2O$, monitored by ^{1}H-NMR were prepared as follows. An amount of 20 mg of $\mathbf{L^G}$ (20.6 μmol) were dissolved in 3 ml of anh. CH_2Cl_2 and 21.1 mg of $Eu(ClO_4)_3 \cdot x\ H_2O$ were dissolved in 10 ml of anh. MeCN. The Eu^{III} concentration ($3.84 \cdot 10^{-3}$ M) was determined by complexometric titration with EDTA in the presence of urotropine and xylene orange [34]. Solns. with $Eu^{III}/\mathbf{L^G}$ ratios of 1.00, 0.66, 0.50, and 0.25 were prepared, stirred at r.t. for 2 h and evaporated to dryness. The solid residues were dissolved in 10 ml of dry CD_3CN in a glove-box under N_2.

The exper. procedures for high-resolution (HR), laser-excited luminescence studies have been published previously [15]. Emission spectra are corrected for the instrumental functions, but HR excitation spectra are not. Quantum yields of the ligand-centered emission were measured relative to quinine sulfate in dil. acidic solution (abs quantum yield: 0.546) [35]. Quantum yields of the metal-centered emission were determined as described in [36] at excitation wavelengths where *i*) the *Lambert-Beer* law is obeyed and *ii*) the absorption of the reference $[Eu(terpy)_3]^{3+}$ (abs. quantum yield 0.013) closely matches that of the sample. Ligand-excitation and emission spectra were recorded on a *Perkin-Elmer LS-50B* spectrometer equipped for low-temp. (77 K) measurements. Elemental analyses were performed by Dr. *H. Eder* (Microchemical Laboratory, University of Geneva).

The molecular-mechanics optimization has been carried out first by means of a MM+ method (RMS gradient = 0.01) followed by a semi-empirical method based on the AM1 Hamiltonian (RMS gradient = 0.1).

Syntheses. 4-Ethynylbenzenamine (**1**). 2-methylbut-3-yn-2-ol (4.61 g, 55 mmol), CuI (0.17 g, 0.91 mmol), and $[PdCl_2(PPh_3)_2]$ (0.65 g, 0.91 mmol) were introduced in a mixture of freshly distilled Et_3N/THF 1:1 (85 ml). The soln. was degassed with N_2 during 15 min at r.t. Then, 4-iodoaniline (10 g, 46 mmol) was added under N_2,

and the mixture was heated at 40° during 3 h. The mixture was filtered, and the filtrate was evaporated under vacuum. The residue was dissolved in Et_2O (100 ml), washed with H_2O (3 × 50 ml) and dried (Na_2SO_4) during 2 h. After solvent evaporation, the brown solid obtained was dried under vacuum (10^{-2} Torr) during 1 h. Toluene was added (30 ml) along with 6 NaOH pellets. The mixture was refluxed during 3 h. After completion of the reaction (TLC; AcOEt/hexane 1:1, R_f (4-ethynylbenzenamine) 0.31), the mixture was filtered, and toluene was evaporated. The resulting black oil was triturated with hexane, and the deep purple solid obtained was crystallized from Et_2O/hexane 1:3 (25 ml) to give a pale yellow solid (2.9 g, 54%). IR (KBr): 1513, 1592 (CC_{aryl}), 1618 ($ArNH_2$), 2230 (C≡CH), 3388, 3487 ($ArNH_2$). ^{1}H-NMR ($CDCl_3$): 2.91 (*s*, CH); 3.77 (*s*, NH_2); 6.55 (*d*, ^3J = 9.48, 2 H); 7.22 (*d*, ^3J = 9.48, 2 H). ^{13}C-NMR ($CDCl_3$): 79.9; 85.2; 112.6; 116.1; 134.9; 146.4. ESI-MS (MeOH): 118.1 ($[M+H]^+$). Anal. calc. for C_8H_7N (117.15): C 82.02, H 6.02, N 11.96; found: C 82.32, H 6.24, N 12.19.

Bis(2-{6-(diethylcarbamoyl)-4-[(4-aminophenyl)ethynyl]pyridin-2-yl}-1-ethylbenzimidazol-5-yl)methane (**2**). The synthon $\mathbf{L^E}$ was synthesized as described in [18][21]; 370 mg of $\mathbf{L^E}$ (0.45 mmol), CuI (7 mg, 0.036 mmol), and $[PdCl_2(PPh_3)_2]$ (13 mg, 0.018 mmol) were introduced in a 1:1 mixture of freshly distilled Et_3N/THF (15 ml). The soln. was degassed during 15 min, and **1** (160 mg, 1.36 mmol, 3 eqs) was added under N_2, and the mixture was further refluxed during 4 h. After solvent evaporation, CH_2Cl_2 (50 ml) was added, and the soln. was washed with H_2O (3 × 50 ml). The org. phase was dried (Na_2SO_4) during 1 h, filtered, evaporated, and dried under vacuum (50°, 10^{-2} Torr). The brown solid obtained was purified by CC (Al_2O_3; CH_2Cl_2/MeOH 99:1 to 94:6) to yield 155 mg (39%) of **2**. Brown pale solid. IR (KBr): 1543, 1589 (Ar), 1618 ($ArNH_2$), 1636 (C=O), 2184 (C≡C), 2871, 2930 (CH_2), 2970 (Me), 3487 ($ArNH_2$). ^{1}H-NMR ($CDCl_3$): 1.12 (*t*, ^3J = 7.15, Me(11′)); 1.32 (*t*, ^3J = 7.12, 3 H, Me(8) or Me(10)); 1.40 (*s*, 2 NH_2); 1.45 (*t*, ^3J = 7.12, 3 H, Me(8) or Me(10)); 3.48 (*q*, ^3J = 7.22, 1 H−C(7) or 1 H−C(9)); 3.66 (*q*, ^3J = 6.99, 1 H−C(7) or 1 H−C(9)); 4.33 (*s*, 1 H, CH_2(b)); 4.84 (*q*, ^3J = 6.82, CH_2(10′)); 7.21 (*s*, H−C(6′)); 7.26 (*s*, H−C(4″), H−C(8″)); 7.39 (br. *d*, H−C(7′)); 7.61 (br. *d*, H−C(5″), H−C(7″)); 7.63 (br. *d*, H−C(5)); 7.72 (*s*, H−C(4′)); 8.53 (br. *d*, H−C(3)). ^{13}C-NMR ($CDCl_3$): 15.1 (C(8) or C(10)); 15.6 (C(8) or C(10)); 17.1 (C(11′)); 40.9 (C(9) or C(7)); 41.8 (C(10′)); 43.2 (CH_2(b)); 44.9 (C(9) or C(7)); 112.6 (C(7′)); 121.9 (C(4′)); 124.8 (C(5)); 126.2 (C(4″), C(8″)); 127.3 (C(6′)); 128.4 (C(3)); 134.8 (C(5″, C(7″)); 88.9, 95.1 (C≡C); 114.2 (2 C); 132.8 (2 C); 135.9, 137.4, 138.6, 144.2, 151.5 (quat. C); 167.6 (C=O). ESI-MS (MeOH): 888.1 ($[M+H]^+$).

Bis(2-{6-(diethylcarbamoyl)-4-[(4-isothiocyanatophenyl)ethynyl]pyridin-2-yl}-1-ethylbenzimidazol-5-yl)-methane ($\mathbf{L^G}$). Compound **2** (100 mg, 0.11 mmol) was dissolved in anh. CH_2Cl_2, di(pyridin-2-yl) thiocarbonate (76.64 mg, 0.33 mmol, 3 equiv.) was added, the soln. was stirred at r.t. overnight and refluxed during 3 h. Solvent evaporation yielded a brown solid, which was recrystallized from a mixture of AcOEt/hexane 40:60 to give 104.8 mg (98%) of $\mathbf{L^G}$. Yellow-brown powder. IR (KBr):31542, 1589 (Ar), 1636 (C=O), 2036 (N=C=S), 2184 (C≡C), 2871, 2930 (CH_2), 2970 (Me). ^{1}H-NMR ($CDCl_3$): 1.10 (*t*, ^3J = 7.16, Me(11′)); 1.29 (*t*, ^3J = 7.14, 3 H, Me(8) or Me(10)); 1.45 (*t*, ^3J = 7.14, 3 H, Me(8) or Me(10)); 3.38 (*q*, ^3J = 7.21, 1 H−C(7) or 1 H−C(9)); 3.62 (*q*, ^3J = 6.84, 2 H, 1 H−C(7) or 1 H−C(9)); 4.30 (*s*, 1 H, CH_2(b)); 4.76 (*q*, ^3J = 6.72, CH_2(10′)); 7.22 (*s*, H−C(6′)); 7.24 (*s*, H−C(4″), H−C(8″)); 7.37 (*d*, ^3J = 8.44, H−C(7′)); 7.53 (*d*, ^3J = 8.44, H−C(5″), H−C(7″)); 7.59 (*d*, ^4J = 1.48, H−C(5)); 7.70 (*s*, H−C(4′)); 8.51 (*d*, ^4J = 1.48, H−C(3)). ^{13}C-NMR ($CDCl_3$): 15.0 (C(8) or C(10)); 15.5 (C(8) or C(10)); 16.1 (C(11′)); 40.3 (C(9) or C(7)); 41.3 (C(10′)); 42.9 (CH_2(b)); 43.5 (C(9) or C(7)); 110.8 (C(7′)); 120.8 (C(4′)); 124.4 (C(5)); 125.9 (C(4″), C(8″)); 126.7 (C(6′)); 127.4 (C(3)); 133.9 (C(5″), C(7″)); 88.6, 94.8 (C≡C); 113.1 (2 C); 132.9 (2 C); 135.6, 137.3, 138.0, 143.7, 150.5 (quat. C); 168.6 (C=O); 155.4 (N=C=S). ESI-MS (MeOH): 486.5 ($[M+2H]^{2+}$), 971.4 ($[M+H]^+$). Anal. calc. for $C_{57}H_{50}N_{10}O_2S_2$ (971.22): C 70.49, H 5.19, N 14.42; found: C 70.68, H 4.98, N 14.65.

Dimethyl 4-[(4-Isothiocyanatophenyl)ethynyl)]pyridine-2,6-dicarboxylate ($\mathbf{L^1}$). Dimethyl 4-[(4-aminophenyl)ethynyl]pyridine-2,6-dicarboxylate (0.25 g, 0.81 mmol), synthesized according to a known procedure [29], was dissolved in dry CH_2Cl_2 (100 ml) and di(pyridin-2-yl) thiocarbonate (0.19 g, 0.81 mmol) was added, and the soln. was stirred overnight at r.t. Solvent evaporation yielded an orange oil, which was purified by CC (CH_2Cl_2 100%): 0.27 g (94%) of $\mathbf{L^1}$. TLC (CH_2Cl_2/MeOH 95:5): R_f 0.71. IR (KBr): 2084 (br.), 1719 (br.), 1507 (br.). ^{1}H-NMR: 8.35 (*s*, H−C(3), H−C(5)); 7.55 (*d*, *J* = 9.8, H−C(3′), H−C(5′)); 7.24 (*d*, *J* = 9.8, H−C(2′), H−C(6′)); 4.03 (*s*, 2 Me). ESI-MS (MeOH): 352.6 (M^+).

Dimethyl 4-[(4-{N′-[5-(Methoxycarbonyl)pentyl]thioureido}phenyl)ethynyl]pyridine-2,6-dicarboxylate ($\mathbf{L^2}$). Compound $\mathbf{L^1}$ (50 mg, 16 mmol) and methyl 6-aminocaproate (29 mg, 0.16 mmol; as its hydrochloride) were dissolved in 20 ml of MeCN; 13.5 mg (0.16 mmol) $NaHCO_3$ were added, and the mixture was stirred 12 h at r.t. before being evaporated and redissolved in CH_2Cl_2. The resultant soln. was washed with 2 × 50 ml of H_2O, dried (Na_2SO_4), and filtered. The yellow solid was dried (50°/10^{-2} Torr) to yield 68 mg (0.12 mmol, 85%) of $\mathbf{L^2}$. ESI-MS (MeOH): 498.1 ($[M+H]^+$). ^{1}H-NMR ($CDCl_3$): 1.38, 1.63, 2.32 (*m*, 2 H, 4 H, 2 H, aliph. CH_2); 3.65

(*s*, MeOCO–C(8″)); 4.03 (*s*, 2 MeOCO(py)); 6.31 (*t*, $^3J = 5.14$, H–N(3″)); 7.27 (*d*, $^3J = 8.44$, H–C(2′), H–C(6′)); 7.59 (*d*, $^3J = 8.8$, H–C(3′), H–C(5′)); 7.95 (br. *s*, H–N(1″)); 8.34 (*s*, H–C(3), H–C(5)). ^{13}C-NMR ($CDCl_3$): 25.00, 26.95, 29.14, 34.40 (aliph. CH_2); 46.00 (1 *Me*OCO(py)); 52.23 (MeOCO–C(8″)); 54.05 (1 *Me*OCO(py)); 86.86, 96.38 (C≡C); 124.72 (C(2′), C(6′)); 130.27 (C(3), C(5)); 134.81 (C(3′), C(5′)); 119.99, 138.51, 149.15 (quat. C); 165.35 (C=O); 181.06 (C=S).

Preparation of the Complexes. The perchlorate salts $Ln(ClO_4)_3 \cdot x\ H_2O$ (Ln = La, Eu, Tb, $x = 2-8$) were prepared from the corresponding oxides (*Rhône-Poulenc*, 99.99%) according to the method in [37]. *Caution:* perchlorate salts combined with org. ligands are potentially explosive and should be handled in small quantities and with the necessary precautions [38].

[Ln_2($\mathbf{L^G}$)$_3$][ClO_4]$_6$·n H_2O (Ln = La, Eu, Tb). A 23-μmol amount of $Ln(ClO_4)_3 \cdot n\ H_2O$ in dry MeCN (1.5 ml) was slowly added to a soln. of $\mathbf{L^G}$ in dry CH_2Cl_2 (1 ml). After stirring at r.t. for 4 h, the soln. was evaporated, the solid residue redissolved in MeCN (1 ml), the soln. was filtered, and Et_2O diffused into the soln. for 3 d. The resulting pale brown microcrystalline aggregates were collected by filtration and dried to give the complexes $[Ln_2(\mathbf{L^G})_3](ClO_4)_6 \cdot n\ H_2O$ (Ln = La, Eu, Tb) in 65–71% yields. The complexes for NMR measurements were prepared by the same procedure but not recrystallized. Elemental analyses are consistent with the above formulation and $n = 4$ (La), 6 (Eu) and 3 (Tb). Anal. calc. for $C_{171}H_{160}Cl_6La_2N_{30}O_{35}S_6$ (3878.26): C 52.96, H 4.16, N 10.83; found: C 53.23, H 4.01, N 11.18. Anal. calc. for $C_{171}H_{162}Cl_6Eu_2N_{30}O_{36}S_6$ (3922.39): C 52.36, H 4.16, N 10.71; found: C 52.09, H 4.31, N 11.01. Anal. calc. for $C_{171}H_{154}Cl_6N_{30}O_{32}S_6Tb_2$ (3864.25): C 53.15, H 4.02, N 10.87; found: C 52.98, H 4.32, N 10.65.

This work is supported through grants from the *Swiss National Science Foundation* and the *Swiss Office for Education and Science* (COST action D18). We thank Dr. *Fabiana Gonçalvès* and *Véronique Foiret* for their help in recording the luminescence data.

REFERENCES

[1] V. W. W. Yam, K. K. W. Lo, *Coord. Chem. Rev.* **1999**, *184*, 157.
[2] P. Caravan, J. J. Ellison, T. J. McMurry, R. B. Lauffer, *Chem. Rev.* **1999**, *99*, 2293.
[3] J. L. Sessler, W. C. Dow, D. Oconnor, A. Harriman, G. Hemmi, T. D. Mody, R. A. Miller, F. Qing, S. Springs, K. Woodbur, S. W. Young, *J. Alloys Compd.* **1997**, *249*, 146.
[4] Z. J. Guo, P. J. Sadler, *Angew. Chem., Int. Ed.* **1999**, *38*, 1513.
[5] I. Hemmilä, T. Ståhlberg, P. Mottram in 'Bioanalytical Applications of Labelling Technologies', Wallac Oy, Turku, 1995.
[6] D. Parker, *Coord. Chem. Rev.* **2000**, *205*, 109.
[7] J.-C. G. Bünzli, N. André, M. Elhabiri, G. Muller, C. Piguet, *J. Alloys Compd.* **2000**, *303/304*, 66.
[8] C. Piguet, J.-C. G. Bünzli, *Chem. Soc. Rev.* **1999**, *28*, 347.
[9] C. Piguet, C. Edder, S. Rigault, G. Bernardinelli, J.-C. G. Bünzli, G. Hopfgartner, *J. Chem. Soc., Dalton Trans.* **2000**, 3999.
[10] C. Edder, C. Piguet, J.-C. G. Bünzli, G. Hopfgartner, *Chem. – Eur. J.* **2001**, *7*, 3014.
[11] S. Petoud, J.-C. G. Bünzli, F. Renaud, C. Piguet, K. J. Schenk, G. Hopfgartner, *Inorg. Chem.* **1997**, *36*, 5750.
[12] G. Muller, J.-C. Bünzli, K. J. Schenk, C. Piguet, G. Hopfgartner, *Inorg. Chem.* **2001**, *40*, 2642.
[13] G. Bernardinelli, C. Piguet, A. F. Williams, *Angew. Chem., Int. Ed.* **1992**, *31*, 1622.
[14] C. Piguet, J.-C. G. Bünzli, G. Bernardinelli, G. Hopfgartner, A. F. Williams, *J. Am. Chem. Soc.* **1993**, *115*, 8197.
[15] N. Martin, J.-C. G. Bünzli, V. McKee, C. Piguet, G. Hopfgartner, *Inorg. Chem.* **1998**, *37*, 577.
[16] M. Elhabiri, R. Scopelliti, J.-C. G. Bünzli, C. Piguet, *J. Am. Chem. Soc.* **1999**, *121*, 10747.
[17] C. C. Wu, M. W. Brechbiel, R. W. Kosak, O. A. Gansow, *Bioorg. Med. Chem. Lett.* **1994**, *4*, 449.
[18] C. Platas, M. Elhabiri, M. Hollenstein, J.-C. G. Bünzli, C. Piguet, *J. Chem. Soc., Dalton Trans.* **2000**, 2031.
[19] J. Hovinen, H. Hakala, *Org. Lett.* **2001**, *3*, 2473.
[20] K. K. W. Lo, D. C. M. Ng, W. K. Hui, K.-K. Cheung, *J. Chem. Soc., Dalton Trans.* **2001**, 2634.
[21] A.-S. Chauvin, R. Tripier, J.-C. G. Bünzli, *Tetrahedron Lett.* **2001**, *42*, 3089.
[22] H. A. Dieck, F. R. Heck, *J. Organomet. Chem.* **1975**, *93*, 259.
[23] K. Sonogashira, Y. Tohda, N. Hagihara, *Tetrahedron Lett.* **1975**, *50*, 4467.
[24] H. Takalo, J. Kankare, E. Hänninen, *Acta Chem. Scand.* **1988**, *B42*, 448.
[25] O. Mongin, A. Gossauer, *Tetrahedron* **1997**, *53*, 6835.
[26] O. Lavastre, L. Olivier, P. H. Dixneuf, S. Sibandhit, *Tetrahedron* **1996**, *52*, 5495.

[27] J. J. Bozell, C. E. Vogt, *J. Am. Chem. Soc.* **1988**, *110*, 2655.
[28] HyperChem, release 5.0, HeperCube Inc., Waterloo, Ontario, Canada, 1996.
[29] C. Platas, C. Piguet, N. André, J.-C. G. Bünzli, *J. Chem. Soc., Dalton Trans.* **2001**, 3084.
[30] F. J. Steemers, W. Verboom, D. N. Reinhoudt, E. B. Vandertol, J. W. Verhoeven, *J. Am. Chem. Soc*. **1995**, *117*, 9408.
[31] F. R. Gonçalves e Silva, R. L. Longo, O. L. Malta, C. Piguet, J.-C. G. Bünzli, *PhysChemChemPhys* **2000**, *2*, 5400.
[32] G. Zucchi, R. Scopelliti, J.-C. G. Bünzli, *J. Chem. Soc., Dalton Trans.* **2001**, 1975.
[33] M. Latva, H. Takalo, V. M. Mukkala, C. Matachescu, J.-C. Rodriguez-Ubis, J. Kankare, *J. Lumin*. **1997**, *75*, 149.
[34] G. Schwarzenbach in 'Complexometric Titrations', Chapman & Hall, London, 1957.
[35] S. R. Meech, D. C. Phillips, *J. Photochem*. **1983**, *23*, 193.
[36] S. Petoud, J.-C. G. Bünzli, T. Glanzman, C. Piguet, Q. Xiang, R. P. Thummel, *J. Lumin*. **1999**, *82*, 69.
[37] J. F. Desreux in 'Lanthanide Probes in Life, Chemical and Earth Sciences. Theory and Practice', Eds. J.-C. G. Bünzli, G. R. Choppin, Elsevier Science Publ. B.V., Amsterdam, 1989 Chapt. 2, p. 43.
[38] W. C. Wolsey, *J. Chem. Educ.* **1973**, *50*, A335.

Received January 24, 2002